nature geoscience

SUPPLEMENTARY INFORMATION

DOI: 10.1038/NGEO2488

Connections between the bulk composition, geodynamics and habitability of Earth

A. M. Jellinek and M. G. Jackson

The Supplementary Information includes the following in a single PDF document:

1. Additional discussion and technical developments for the geochemical, geodynamic and climate models, including references.
2. A figure (Supplementary Figure 1) that explores relationships between mean surface temperature, volcanic greenhouse and solar forcing over Earth's history.
3. A figure (Supplementary Figure 2) that investigates the tectonic regime of a planet (mobile lid, episodic, stagnant lid and "multi-mode") as a function of mantle temperature for a range of lithospheric yield stresses and radiogenic heating levels.
4. Supplementary Table 1 provides a summary of bulk silicate Earth compositions for a non-chondritic planet. Compositions for a hidden early enriched reservoir are also provided, and are given as a function of the mass of this reservoir.

Supplementary Information:

Survival of the early depleted reservoir in the modern mantle.

Evidence for the survival of undifferentiated portions of the early depleted reservoir in the modern mantle (Fig. 1, Panels B and C) is suggested in some hotspot lavas. Most convincing in this regard, lavas with the highest, most primitive $^{3}He/^{4}He$ have primitive Pb-isotopic compositions near the terrestrial geochron—the locus of data in $^{207}Pb/^{204}Pb$ versus $^{206}Pb/^{204}Pb$ that have had undisturbed U/Pb ratios for the age of the Earth—and primitive (but not chondritic) $^{143}Nd/^{144}Nd$ ratios that match the early depleted reservoir (i.e., 0.5130 ± 0.0001)[12,15] predicted by its higher Sm/Nd ratio. This is consistent with recent discoveries of $^{129}Xe/^{130}Xe$ isotope anomalies in different mantle reservoirs[74], including the mid-ocean ridge basalt and high $^{3}He/^{4}He$ mantle reservoirs, which argues for early formation (<100 Myr following accretion) of the high $^{3}He/^{4}He$ mantle. This timescale overlaps with the timeline for early depleted reservoir formation (<20 to 30 Myr after accretion) from ^{146}Sm-^{142}Nd systematics. If high $^{3}He/^{4}He$ lavas represent melts of the early depleted reservoir, they sample a reservoir that formed early and survived ~4.5 Ga of mantle convection before being melted to form hotspots and large igneous provinces[12,15]. Dynamic models suggest that portions of the mantle can survive unscathed over such times scales[75].

The composition of the early enriched reservoir.

The composition of the early enriched reservoir (which may reside in space or at the bottom of the mantle), as shown in Fig. 2, is calculated as a function of its mass using

the following mass balance equation: $[x]_{EDR} \cdot M_{EDR} + [x]_{EER} \cdot M_{EER} = [x]_{BSE} \cdot M_{BSE}$, where [x] is the concentration of element x in the early depleted reservoir (EDR)[20], the early enriched reservoir (EER; this study), and chondrite-based bulk silicate Earth (BSE)[3], and M represents the mass of each reservoir (after ref. 9). The mass of the early enriched reservoir (M_{EER}) is unknown, but its composition is shown for several different possible mass fractions of the bulk silicate Earth in Fig. 2. The most highly incompatible element concentrations in the EER are similar to estimates for the bulk composition of the continental crust[76] when the mass of the EER is 0.5% of the mass of the silicate Earth (which is, incidentally, approximately the same mass as the modern continental crust). In this calculation, the composition of the early enriched reservoir, determined by mass balance, depends on the composition of the early depleted reservoir (several distinct compositions for the early depleted reservoir exist[11,16,20,77,78]), but we use the estimate from ref. 20 and the initial chondrite-based bulk silicate Earth composition from ref. 3. Extraction of the EER from the chondrite-based mantle generated the early depleted reservoir ("first melt extraction" in Fig. 2), and subsequent extraction of continental crust from the early depleted reservoir formed the depleted MORB mantle ("second melt extraction" in Fig. 2), for which several compositional estimates exist[10,79,80].

Volcanic forcing, chemical weathering and steady-state climate.

Earth's climate variability over long time scales is modulated by the radiative greenhouse forcing resulting from a balance between the rate at which CO_2 is injected into the atmosphere from volcanoes, F_{outgas}, and the time scale, t_w, over which CO_2 is

drawn down by primarily by silicate weathering reactions in soils to ultimately form seafloor carbonate[60,81,82]. Average chemical weathering rates depend on factors including the surface temperature ($T_{surface}$) and precipitation (surface runoff)[82,83], but also on the rate at which weatherable soils are produced through mechanical erosion processes[84] governed, in part, by the rate at which plates collide with continents to build mountains[85]. Gradual cooling in a mantle with less radiogenic heat (i.e., the collisional erosion case explored here) produces large increases in Earth's mantle viscosity, $\mu(T_{mtl})$, which reduces rates of subduction and the flux of volcanic outgassing[60]. This effect on the tectonic regime can influence the strength of the mechanical and chemical weathering CO_2 sink through associated changes in processes like mountain building and related precipitation at convergent plate boundaries[85], as well as by modulating additional atmospheric CO_2 drawdown through seafloor weathering processes[60].

We explore changes in volcanic degassing, atmospheric pCO_2, etc., relative to present day conditions (i.e., "now", Fig. 3) that relate to the thermal history of the mantle. To parameterize a chemical weathering sink we fix the precipitation rate to the present-day average and combine the well-known Arrhenius temperature dependence of the Urey weathering reactions[83,86] with a novel parameterization for mechanical weathering efficiency drawn from recent field measurements[84] and models for the self-similar growth and erosion of orogens at convergent plate boundaries[85]. We do not include effects of mechanical weathering by glaciers, as such effects are challenging to parameterize. We assume that accretion rates at active orogens are proportional to the rate of mantle overturning. We also assume for simplicity that the majority of rocks undergoing mechanical and chemical weathering at active orogens are granitic (relative to today we

add no new surface area of basalt, which would enhance the drawdown of atmospheric CO_2). We do not include additional sinks related to seafloor weathering and organic carbon burial, which are clear directions for future work under the changing tectonic and volcanic conditions we envisage. Seafloor weathering efficiency depends weakly on factors including ocean pH[87], and more strongly on crustal production rates at mid-ocean ridges[60] as well as mean ocean temperature and composition[88]. An organic carbon burial sink will have a strength that depends, in part, on the mechanical/chemical weathering-limited delivery of phosphate to continental shelves[89], which will have a surface area that depends on mean sea level (i.e., which is related to the mantle thermal regime) and the total surface area of continents. Finally, we do not include additional novel contributions to the volcanic forcing related to, for example, Earth's evolving inventory of subducted carbonate rocks, which substantially increase the CO_2 outgassing from arc volcanoes in Earth's relatively recent past[58].

We assume a constant alkalinity ocean saturated in calcium carbonate[63,81] and a self-similar growth of collisional orogens with a constant erosion efficiency[85,90] to constrain the steady state atmospheric $(pCO_2 / pCO_{2,now}) \propto (F_{outgas}/ F_{outgas,now})^2 (t_{w,} / t_{w,now})$, where $(F_{outgas} / F_{outgas,now}) \propto (\mu_{mtl,now} / \mu_{mtl})$ and $(t_{w,} / t_{w,now})$ is approximately proportional to $[\mu(T_{mtl,now}) / \mu(T_{mtl})]^{ß} \exp[(G_{eff} / (RT_{surface}))(1-(T_{surface}/T_{surface,now}))]$, where ß ≈ 0.4. Here G_{eff} is an effective activation energy for the kinetics of chemical weathering of granites[84] and R is the gas constant. We neglect potentially important changes in rainfall and runoff related to changes in mean atmospheric temperature and to orographic effects related to changes in the global distribution and intensity of mountain building processes. Chemical weathering rates (and CO_2 draw down) increase with $T_{surface}$ and resurfacing rates (which,

in turn, increase with increasing T_{mtl} in Fig. 3). Here, the surface temperature change ($T_{surface}/T_{surface,now}$) used in the weathering calculation is determined from a global radiative energy balance assuming a CO_2-$H_2O_{(v)}$ atmosphere with Earth's current nitrogen pressure[58]. For simplicity, we fix the solar constant to the present day value and potentially overestimate the surface temperature back in time (Supplementary Figure 1). However, although weathering reactions are faster in a warmer world (implying that we overestimate weathering rates in the past and underpredict the rise in pCO_2), complex and large variations in the precipitation regime with the formation and breakup of supercontinents[91-93] over the last 2 Ga may mitigate these effects to some degree[93]. Our model is, however, intended only to be heuristic and show a potential trend in pCO_2 related to an explicit prediction for changes in the volcanic delivery of CO_2 to the atmosphere as described above.

A frozen, fried or clement (habitable) Earth?

Earth's climate at any time depends on a global balance between the solar heat flux absorbed at the surface and the outgoing long wavelength radiation (OLR) emitted to space, which depends mostly on the mean surface temperature $T_{surface}$ and greenhouse gases such as CO_2:

$$S_0(t)(1-\alpha_{surface})(1-\alpha_{sky}) = OLR(T_{surface}, pCO_2) \qquad (1)$$

where $S_0(t)$ is the influx of solar heating over time and $a_{surface}$ and a_{sky} are the mean surface and atmospheric albedos. Greenhouse forcing can be characterized in terms of the fraction of OLR emitted from Earth's surface to space, where 1 and 0 correspond to the

no- and opaque atmosphere limits, respectively (Supplementary Figure 1). In typical zonal energy balance models that explore how changing solar or greenhouse conditions affect the advance or retreat of glaciers and the potential for global glaciation, equation 1 is modified[94] to include interzonal (meridional) heat transfer and the potential for zonal changes in the planetary albedo related to low altitude clouds and aerosols[58,95] (Supplementary Figure 1):

$$S_0(t)(1-\alpha_{surface,i})(1-\alpha_{sky,i}) - OLR(T_i, pCO) = k(T_i - T_{surface,mean}) \qquad (2)$$

where the subscript *i* refers to zone *i*, and *k* is the meridional heat transfer coefficient that is tuned to present-day ocean stirring conditions[94], and $T_{surface,mean}$ is the mean surface temperature over all zones. The mean surface albedo in each latitude band depends on areal fraction of, e.g., land/sea/ice, as well as on temperature. In particular, if zonal temperatures drop below a critical value, then $a = a_{ice}$ (ref. 58). If the ice line advances from the poles to about 30º latitude (about 50% of the surface area of the planet), global glaciation will occur through a well-known ice-albedo feedback[58,94].

For a present day continental distribution and $a_{sky} = 0.2$, surface temperatures for different solar constants back through time (colored lines in Supplementary Figure 1) vary with the strength of the greenhouse forcing. If the intensity of solar insolation is fixed at the present-day value, a continuously increasing supply of volcanic CO_2 favors a world free of glaciers over the majority of Earth's history (dash-dotted arrow along orange line). By contrast, if the intensity of volcanic greenhouse forcing is fixed, a steady decline in insolation back in time predicts global glaciation before 3.5 Ga (dotted arrow), which is inconsistent with geological data and an example of the so-called "Faint Young Sun Paradox". Hysteresis is an intrinsic property of the way in which a model Earth

might recover from this solution: to recover a clement climate, pCO_2 must rise substantially above the levels that characterized entry into global glaciation[96].

We perform calculations with equation 2 assuming a present day average surface and planetary albedo (Supplementary Figure 1, solid colored lines) as well as calculations for a water planet with lower $a_{surface}$ (Supplementary Figure 1, dashed colored lines), which may be a better analog for an Archean Earth with few continents (Supplementary Information). These situations provide end-members: A present-day continental configuration leads to an overestimate of the effects of the decline in solar insolation on Earth's climate and a water planet gives an underestimate[58,95]. We do not explore potential reductions in a_{sky} related to an absence of microbial aerosols[95] or to uncertain changes in the volcanic production of dust and aerosols. We also make no allowance for effects related to probable variations in the efficiency of meridional heat transport in the oceans[96]. These calculations are intended to provide qualitative insight.

Bearing in mind the limitations of our calculations, the form of the steady increase in greenhouse forcing backwards in time (suggested by Fig. 3) is a previously unrecognized tectonically-driven effect that will mitigate effects of a declining solar flux. Acting potentially in combination with water vapor and other greenhouse gases[97] and plausibly concomitant increases in greenhouse forcing from high atmospheric clouds[58], our picture presents a new contribution to the discussion of how to resolve the faint young sun paradox, which is also consistent varied, albeit contentious proxy data for pCO_2 in the Archean[98-103]. We show one (of many) possible partial-ice solution (dashed arrow) to illustrate this possibility (Supplementary Figure 1).

As a further remark, time-dependent changes in plate motions, including episodic behavior in the Precambrian[66] and supercontinental cycles[93], will perturb this basic climate picture, consistent with observed long-period climate oscillations[61,63,99,104-106]. This simple climate exercise serves to demonstrate that greater greenhouse forcing prior to 3.5 Ga, as predicted by our model, may help to avert an early globally-glaciated world.

Finally, stepping back from a discussion of Earth's history, extreme and long-term (e.g., 10^9 year) oscillations in volcanic forcing, potentially characteristic of episodic tectonic modes[64] varying from "stagnant lid" regimes to "mobile lid" regimes (Supplementary Figure 2 and discussion below) may lead to protracted ice-free states or to global glaciations. Conditions favoring habitability can occur, but are likely to be highly time-dependent.

Chondritic versus non-chondritic heat production and the tectonic regime of planets.

Reduced radiogenic heating in the Earth (as predicted by the collisional erosion model) may have consequences for the evolution of the tectonic regime of the planet. In Supplementary Figure 2, two solid red lines depict cooling laws for different tectonic regimes. The upper solid red line is the mobile lid convecting cooling law used to model the thermal history in Fig. 3, and reflects the specified contributions from large and small plates. The lower solid red line is a typical stagnant lid convective cooling law, and is appropriate for one-plate planets (e.g., present-day Venus). To maintain a mobile lid regime, mantle convective stresses imparted to the lithosphere (solid black line in Supplementary Figure 2) must exceed the strength of a plate[65,107] and act on a time scale that is small in comparison to the time scale for healing of a plate boundary[108-110]. Recent

work also shows that the history of a planet's tectonic regime can influence the likelihood of the current regime as well as the resilience of this regime in the future[67,111,112].

Convective stresses decline strongly as the mantle viscosity drops with increasing temperature[65,66]. At steady-state, mantle temperature is set by a balance between radiogenic heat production and the heat lost as a result of plate resurfacing[113] (large-dashed red line, representing the collisional erosion case; Supplementary Figure 2). For our thermal history (Fig. 3) —where the insulating effect of continents supplies the effect of 7 TW of additional warming to a mantle[114] with 7 TW of internal radiogenic heating[20]—T_{mtl}=1350 ^{o}C (red/white circle) and present-day convective stress levels are well within a regime favoring a mobile lid mode consistent with present-day Earth (though episodic behavior is permitted[65-67,111]) (black/white circle).

As a thought experiment, if we impulsively increase the heating rate by 5 TW towards a chondritic value (small-dashed red line, Supplementary Figure 2), without adjusting the convective regime in any way, the internal temperature climbs to a new steady-state value (red/yellow circle), convective stresses fall well into a regime favoring stagnant lid or episodic modes (black/yellow circle), and our model Earth transitions on to a cooling path governed by stagnant lid convection (black/red circle). In reality, higher heat production will also change the relative contributions of large versus small plates-to the thermal history calculation with more plausible increases in mantle temperature of perhaps 50-100 ^{o}C[52] (i.e., our thought experiment produces unrealistically high temperatures). Nevertheless, the point of this exercise to illustrate that, compared to a collisional erosion-based bulk silicate Earth, enhanced heat production for a chondrite-based bulk silicate Earth composition will drive the system away from present-day

mobile lid behavior towards a greater likelihood for episodic- or stagnant lid-style tectonics, and thus toward non-clement climate regimes.

References

74. Mukhopadhyay, S. Early differentiation and volatile accretion recorded in deep-mantle neon and xenon. *Nature* **486**, 101-104 (2012).

75. Brandenburg, J.P., Hauri, E.K., van Keken, P.E. & Ballentine, C.J. A multiple system study of the geochemical evolution of the mantle with force-balanced plates and thermochemical effects. *Earth Planet. Sci. Lett.* **276**, 1–13 (2008).

76. Rudnick, R.L. & Gao, S. Composition of the continental crust, in Treatise on Geochemistry, vol. 3, The Crust, edited by R. L. Rudnick, pp. 1–64, Pergamon, New York (2003).

77. Zhang, Y. Quantification of the elemental incompatibility sequence, and composition of the "superchondritic" mantle. *Chem. Geol.* **369**, 12-21 (2014).

78. White, W.M. *Geochemistry*. Wiley-Blackwell (2013).

79. Salters, V.J.M. & Stracke, A. Composition of the depleted mantle. *Geochem. Geophys. Geosyst.* **5**, Q05004 (2004).

80. Workman, R.K. & Hart, S.R. Major and trace element composition of the depleted MORB mantle (DMM). *Earth Planet. Sci. Lett.* **231**, 53-72 (2005).

81. Schrag, D.P., Berner, R., Hoffman, P.F. & Halverson, G.P. On the initiation of a snowball Earth. *Geochem. Geophys. Geosyst.* **6** (2002). doi: 10.1029/2001GC000219

82. Berner, R.A. & Kothavala, Z. GEOCARB III: a revised model of atmospheric CO_2 over Phanerozoic time. *American J. Sci.* **301**, 182-204 (2001).

83. Walker, J.C.G., P.B. Hays & J.F. Kasting. A negative feedback mechanism for the long-term stabilization of Earth's surface temperature, *J. Geophys. Res.*, **86**, 9776-9782 (1981).

84. Riebe, C.S., Kirchner, J.W. & Finkel, R.C. Erosional and climatic effects on long-term chemical weathering rates in granitic landscapes spanning diverse climate regimes. *Earth Planet. Sci. Lett.* **224**, 547-562 (2004).

85. Roe, G. H., Whipple, K.X. & Fletcher, J.K. Feedbacks among climate, erosion, and tectonics in a critical wedge orogen. *Am. J. Sci.* **308**, 815-842 (2008).

86. Dessert, C., *et al.* Erosion of Deccan Traps determined by river geochemistry: Impact on the global climate and the $^{87}Sr/^{86}Sr$ ratio of seawater. *Earth Planet. Sci. Lett.* **188**, 459-474 (2001).

87. Caldeira, K. Long-term control of atmospheric carbon dioxide: low-temperature seafloor alteration of terrestrial silicate weathering? *Am. J. Sci.* **295**, 1077-1114 (1995).

88. Coogan, L.A. & Gillis, K.M. Evidence that low-temperature oceanic hydrothermal systems play an important role in the silicate-carbonate weathering cycle and long-term climate regulation. Geochem. Geophys. Geosyst. 14, 1771–1786 (2013).

89. Bjerrum, C. J., Bendtsen, J., & Legarth, J. J. F. Modeling organic carbon burial during sea level rise with reference to the Cretaceous. *Geochem., Geophys., Geosyst.*, **7**. (2006) DOI: 10.1029/2005GC001032

90. Whipple, K. X., & Meade, B. J. Controls on the strength of coupling among climate, erosion, and deformation in two-sided, frictional orogenic wedges at steady state. *J. Geophys. Res.: Earth Surface* **109**. F01011 (2004).

91. Donnadieu, Y., Pierrehumbert, R., Jacob, R., & Fluteau, F. Modelling the primary

control of paleogeography on Cretaceous climate. *Earth Planet Sci Lett.* **248**, 426-437 (2006).

92. Le Hir, G., Donnadieu, Y., Goddéris, Y., Pierrehumbert, R.T., Halverson, G.P., Macouin, M., Nedelec, A. & Ramstein, G. The snowball Earth aftermath: Exploring the limits of continental weathering processes. *Earth Planet. Sci. Lett.* **277**, 453-463 (2009).

93. Jellinek, M., Pierrehumbert, R., Turchyn, A.V., & Lenardic, A. Supercontinental Cycles and the Tectonic Modulation of Earth's Climate. Abstract T33J-06 presented at 2012 Fall Meeting, American Geophysical Union, San Francisco, Calif., 3-7 Dec.

94. Budyko, M. I. The effect of solar radiation variations on the climate of the earth. *Tellus*, **21**, 611-619 (1969)

95. Rosing, M.T., Bird, D.K., Sleep, N.H., & Bjerrum, C.J. No climate paradox under the faint early Sun. *Nature* **464**, 744-747 (2010).

96. Ferreira, D., Marshall, J., & Rose, B., 2011, Climate determinism revisited: multiple equilibria in a complex climate model. *J. Climate* **24**, 992-1012, doi: 10.1175/2010JCL13580.1

97. Haqq-Misra, J. D., Domagal-Goldman, S.D., Kasting, P.J. & Kasting, J.F. A revised, hazy methane greenhouse for the Archean Earth. *Astrobiology* **8**, 1127-1137 (2008).

98. Rye, R., Kuo, P.H., & Holland, H.D. Atmospheric carbon dioxide concentrations before 2.2 billion years ago. *Nature* **378**, 603-605 (1995).

99. Lowe, D.R., & Tice, M.M. Geologic evidence for Archean atmospheric and climatic evolution: Fluctuating levels of CO_2, CH_4, and O_2 with an overriding tectonic control. *Geology* **32**, 493-496 (2004).

100. Goldblatt, C., & Zahnle, K.J. Faint young Sun paradox remains. *Nature* **474**, E1-E1.

(2011).

101. Reinhard, C.T., & Planavsky, N.J. Mineralogical constraints on Precambrian pCO_2. *Nature* **474**, E1-E1 (2011).

102. Dauphas, N., & Kasting, J.F. Low pCO_2 in the pore water, not in the Archean air. *Nature*, *474*, E1-E1 (2011).

103. Rosing, M.T., Bird, D.K., Sleep, N.H., & Bjerrum, C.J. Rosing, Bird, Sleep & Bjerrum reply. *Nature* **474**, E1-E1 (2011).

104. Royer, D.L., Berner, R.A., Montañez, I.P., Tabor, N.J. & Beerling, D.J. CO_2 as a primary driver of Phanerozoic climate. *GSA today* **14**, 4-10 (2004).

105. Zachos, J., Pagani, M., Sloan, L., Thomas, E. & Billups, K. Trends, rhythms, and aberrations in global climate 65 Ma to present. *Science* **292**, 686-693 (2001).

106. Hansen, J., Sato, M., Russell, G., & Kharecha, P. (2013). Climate sensitivity, sea level and atmospheric carbon dioxide. *Philos. T Roy. Soc A* **371**, 20120294 (2001).

107. Moresi, L., & Solomatov, V. Mantle convection with a brittle lithosphere: thoughts on the global tectonic styles of the Earth and Venus. *Geophys. J. Int.* **133**, 669-682 (1998).

108. Lenardic, A., Jellinek, A.M., & Moresi, L.N. A climate induced transition in the tectonic style of a terrestrial planet. *Earth Planet. Sci. Lett.* **271**, 34-42 (2008).

109. Landuyt, W., & Bercovici, D. Variations in planetary convection via the effect of climate on damage. *Earth Planet. Sci. Lett.* **277**, 29-37 (2009).

110. Foley, B. J., Bercovici, D. & Landuyt, W. The conditions for plate tectonics on super-Earths: inferences from convection models with damage. *Earth Planet. Sci. Lett.* **331**, 281-290 (2012).

111. Lenardic, A., & Crowley, J.W. On the notion of well-defined tectonic regimes for terrestrial planets in this solar system and others. *Astrophys. J.* **755**, 132 (2012). doi:10.1088/0004-637X/755/2/132, 2012

112. Bercovici, D., & Ricard, Y. Plate tectonics, damage and inheritance. *Nature* **508**, 513-516 (2014).

113. Tozer, D. C. The present thermal state of the terrestrial planets. *Phys. Earth Planet. Int.* **6**, 182-197 (1972).

114. Lenardic, A., Cooper, C.M., & Moresi, L. (2011). A note on continents and the Earth's Urey ratio. *Phys. Earth Planet. Int.***188**, 127-130.

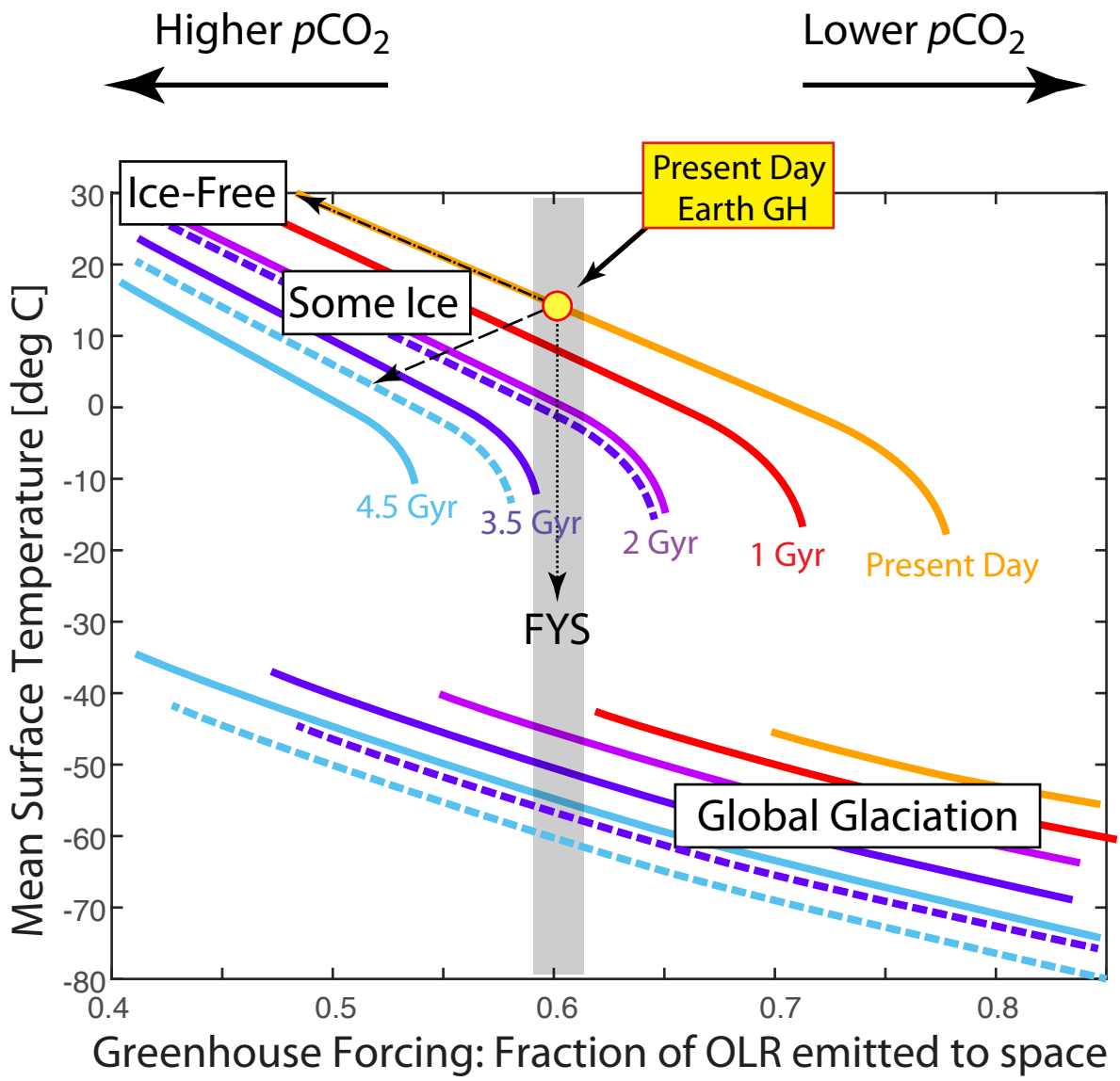

Supplementary Figure 1. Mean surface temperature as a function of greenhouse forcing leads to ice-free, partial-ice and global glaciation solutions. Surface temperatures for different solar constants back through time (colored lines) vary with the strength of the greenhouse forcing. Solid lines assume an albedo based on the present-day distribution of continents. Dashed lines of the same color assume no continental surface area (i.e., water worlds) and may better capture Archean Earth. The grey region defines present-day greenhouse forcing, and the present-day Earth plots on the yellow/red circle. If solar insolation is fixed at the present-day value and if carbon dioxide is increased, an ice-free solution is favored (dash-dotted arrow). If the greenhouse forcing is fixed, reduced insolation back in time (dotted arrow) predicts global glaciation before 3.5 Ga. Dashed arrow shows one (of many) possible partial ice solution assuming the atmosphere is saturated in water vapor. A dry atmosphere gives a global glaciation solution (not shown).
OLR is outgoing long wavelength radiation, FYS is faint young sun, GH is greenhouse.

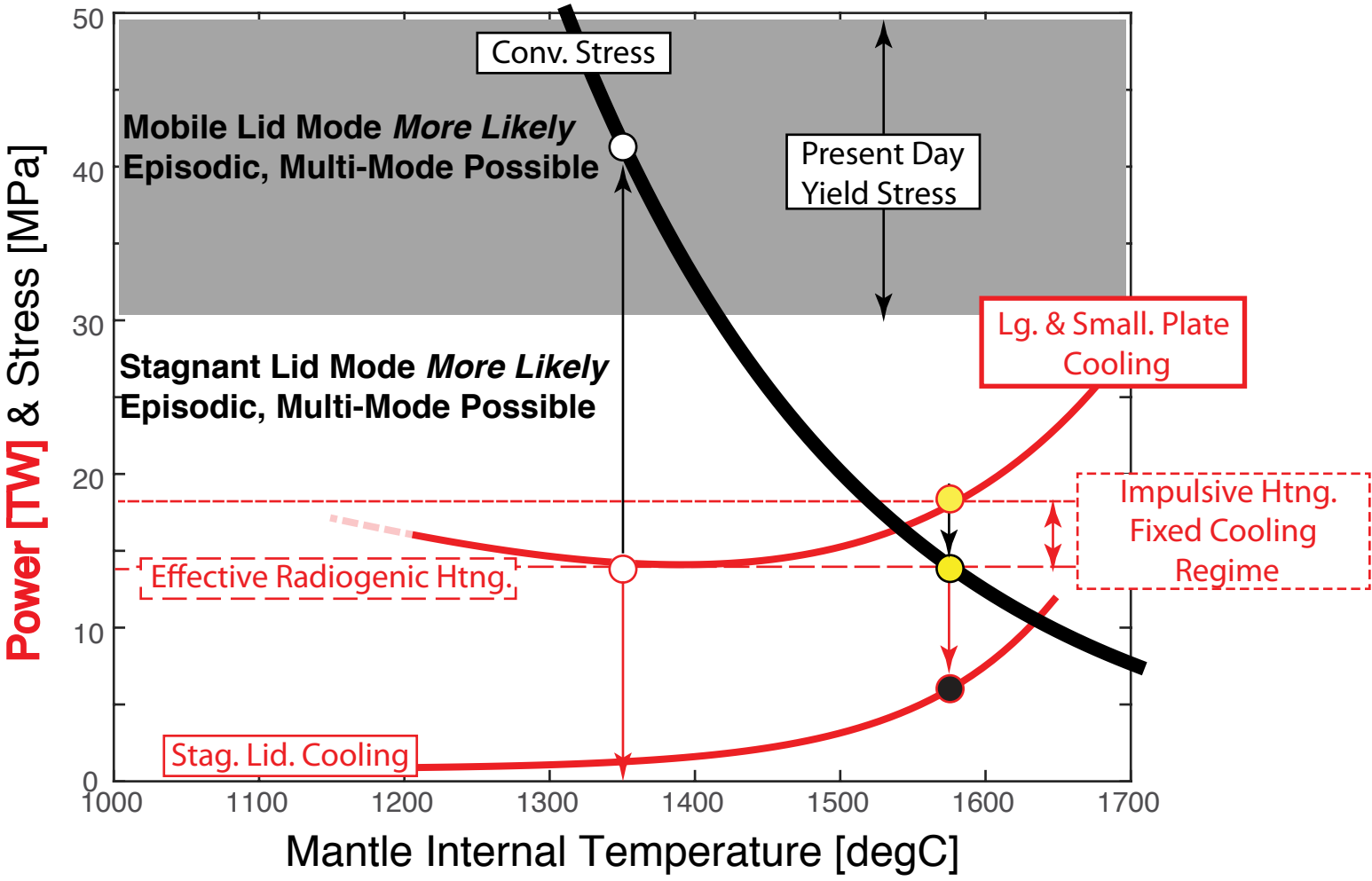

Supplementary Figure 2. The two solid red lines depict cooling laws for different tectonic regimes. The upper solid red line is the mobile lid convecting cooling law used to model the thermal history in Fig. 3, and reflects contributions from large (23%) and small plates (77%); the lower solid red line is a typical stagnant lid convective cooling law, and is appropriate for one-plate planets. We assume vigorous mantle convection will no longer occur for T_{mtl}<1200 ºC (faded dashed extension to heavy red line). Convective stresses imparted to the lithosphere are represented by a solid black line, and the present-day yield stress is indicated by the grey region. In the collisional erosion case, heating (i.e., 14 TW of "effective radiogenic heating" in the mantle, which includes 7 TW of mantle-derived radiogenic heating and the warming effect of 7 TW of thermal insulation from the continents) is represented by the large-dashed red line, which intersects convective cooling scaling to give the present-day mantle potential temperature at the red/white circle; at this temperature, stress levels are within a regime favoring mobile lid tectonic regime (black/white circle) consistent with the present-day Earth. A 5 TW impulsive mantle heating experiment is represented by the small-dashed line, the mantle temperature climbs to a new steady-state (yellow/red circle); at this (unrealistically high, see text) temperature, stress levels are in a regime that favors a stagnant lid (yellow/black circle) and the model Earth transitions to a cooling path that favors stagnant lid convection (red/black circle).

Supplementary Table 1. Concentration of U, Th and K and radiogenic heat production for several geochemical reservoirs, including several estimates for the early depleted reservoir (EDR) and early enriched reservoir (EER); continental crust and chondrite-based bulk silicate Earth compositions shown for reference.

	EDR JJ13	EDR Z14	EDR W13	EDR OP08	EDR CB08	EER (this study) 0.5% of BSE	Continental Crust RG03	Chondrite-based BSE MS95
Th (ppm)	0.0545	0.047	0.0628	0.044	0.0475	5.05	5.6	0.0795
U (ppm)	0.0140	0.013	0.0164	0.012	0.0135	1.28	1.3	0.0203
K (ppm)	166	158	219	120	153	14902	15606	240
Radiogenic heat production (TW)	13.8	12.5	16.5	11.1	12.6	6.3	7.2	20

JJ13=ref. 20; W13=ref. 78; Z14=ref. 77; OP08=ref. 16; CB08=Ref. 11; MS95=Ref. 3; RG03=Ref. 76

The concentration of incompatible trace elements in the EER depends on its mass (given as mass fraction of the BSE), and a range of concentrations are calculated given the mass balance formula in the Supplementary Information and the EDR composition from ref. 20.

The total radiogenic heat prodution shown for the EDR compositional estimates assumes that the EDR comprises 100% of the BSE.